© Copyright 2020. WILEY-VCH GmbH.

# Supporting Information

## Bidimensional H-Bond Network Promotes Structural Order and Electron Transport in BPyMPMs Molecular Semiconductor

*Antonio De Nicola,* Andrea Correa, Andrea Giunchi, Luca Muccioli, Gabriele D'Avino, Junji Kido and Giuseppe Milano*

Dr. Antonio De Nicola, Prof. G. Milano, Prof. J. Kido
Frontier Center for Organic Materials (FROM), Yamagata University,
4-3-16 Jonan, Yonezawa, Yamagata 992-8510, Japan
E-mail: adenicola@yz.yamagata-u.ac.jp

Prof. A. Correa
Department of Chemistry, University of Napoli Federico II,
Complesso di Monte S. Angelo, 80126, Napoli, Italy

Prof. L. Muccioli, Dr. A. Giunchi
Department of Industrial Chemistry "Toso Montanari", University of Bologna,
40136 Bologna, Italy

Dr. G. D'Avino
Grenoble Alpes University, CNRS, Grenoble INP, Institut Néel,
25 rue des Martyrs, 38042 Grenoble, France

Prof. G. Milano
Department of Chemisty and Biology "Adolfo Zambelli", University of Salerno,
*84084 Fisciano, Italy*

# Table of Content

**TABLE OF CONTENT** ..... **2**

**1. ATOMISTIC MODELS OF BPYMPM MOLECULES** ..... **3**

**2. ADDITIONAL ANALYSIS** ..... **6**

2.1 CRYSTALLINE SYSTEM OF B4PYPTZ ..... 6

2.2 THIN FILM PREPARATION ..... 8

2.3 HYDROGEN BONDS(H-BONDS): ADOPTED CRITERIA AND ADDITIONAL ANALYSIS ..... 10

2.4 ADDITIONAL ANALYSIS ON BULK AND MOLECULAR STRUCTURES ..... 13

2.5 ADDITIONAL CHARGE TRANSPORT CALCULATIONS ..... 14

**REFERENCES:** ..... **17**

## 1. Atomistic Models of BPyMPM Molecules

The bonded and non-bonded parameters of B4, B2 and B4PyPTZ were taken from the general all atom OPLS force field.[1],[2] The force field parameters for the dihedral angles T1 and T2 (see Figure 1 of the main text) have been re-optimized by using DFT calculations. In the following the functional forms of bonded and non-bonded interactions are reported together with the adopted parameters (Table S1-S5). In Figure S1, the partial charge attribution and atom type definition are reported. For simplicity, only B4 molecular structure is used to show atom definitions and charge attribution. However, unless the different position of nitrogen atoms in pyridine rings, the scheme reported in Figure S1 is valid also for B2 molecules.

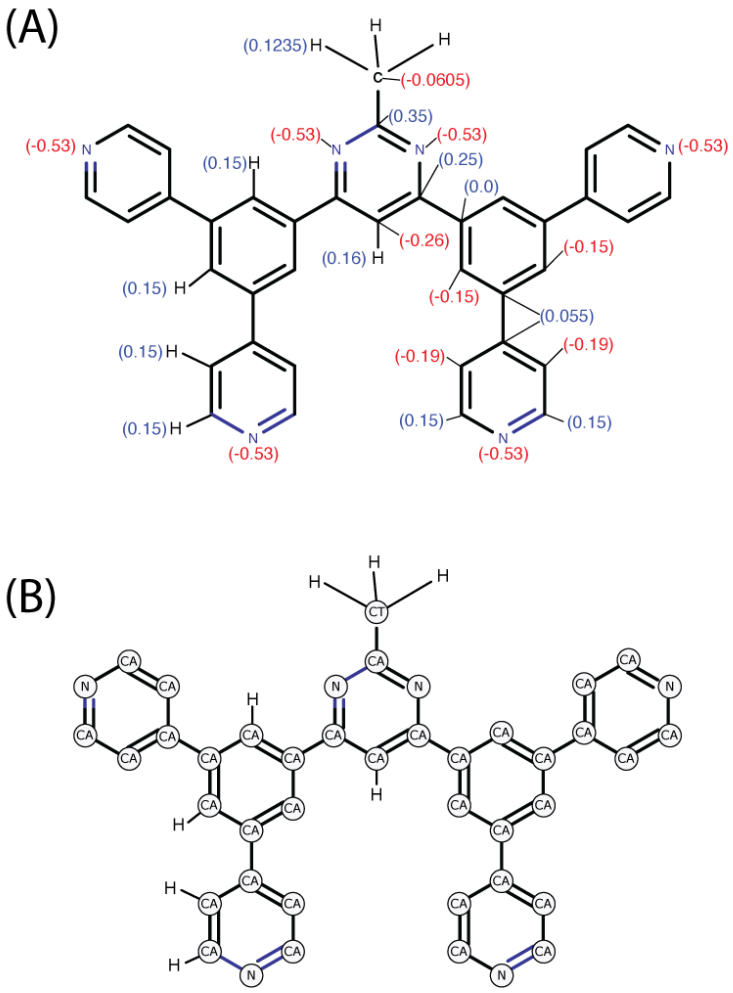


**Figure S1.** (A) Partial charge attribution to atoms. The molecule is ideally divided in two parts. On the right side of the molecule, charges of carbon atoms are reported. Besides, on the left side of the molecule the charge attribution is reported for hydrogen atoms. Only atoms having different charge values and peculiar position in the molecule are reported. (B) Atom type attribution. For both, bonded and non-bonded interactions the labelled types are used to refer to a specific atom type.

### *1.1 Non-bonded interactions*[2]

$$u(r_{ij}) = 4\epsilon\left[\left(\frac{\sigma}{r}\right)^{12} - \left(\frac{\sigma}{r}\right)^{6}\right] + \left(\frac{1}{4\pi\epsilon_0}\right)\left(\frac{q_i q_j}{r_{ij}}\right) \text{(S1)}$$

**Tab. S1**: Interaction non-bonded terms

| **Atom Type** | $\boldsymbol{\sigma}$ (Ang.) | $\boldsymbol{\epsilon}$ (kcal/mol) |
|---|---|---|
| CT | 3.50 | 2.76144 |
| H(CT) | 2.50 | 1.25520 |
| H(CA) | 2.42 | 1.25520 |
| CA | 3.50 | 2.92880 |
| N | 3.25 | 7.11280 |

### *1.2 Bond Interactions*[2]

$$V_{bond} = \frac{K_{bond}}{2}(r_{ij} - r_0)^2 \quad \text{(S2)}$$

**Tab. S2**: Interaction Bond Terms

| **Bond Type** | $\boldsymbol{K_{bond}}$ (kcal/mol/Ang.$^2$) | $\boldsymbol{r_0}$ (Ang.) |
|---|---|---|
| CT-CA | 265.2656 | 1.510 |
| CT-H(CT) | 284.5120 | 1.090 |
| CA-N | 404.1744 | 1.339 |
| CA-CA (in ring) | 392.2542 | 1.400 |
| CA-CA (connecting two rings) | 322.1680 | 1.460 |
| CA-H(CA) | 307.1056 | 1.080 |

$$V_{angle} = \frac{K_{angle}}{2}(\theta_{ij} - \theta_0)^2 \quad \text{(S3)}$$

**Tab. S3**: Interaction Angle Terms

| **Angle Type** | $\boldsymbol{K_{angle}}$ (kcal/mol/rad$^2$) | $\boldsymbol{\theta_0}$ (deg.) |
|---|---|---|
| CA-CT-H(CT) | 292.880 | 109.5 |
| CT-CA-N | 585.760 | 115.5 |
| CA-N-CA | 585.760 | 117.0 |
| N-CA-CA | 585.760 | 124.0 |
| CA-CA-CA | 527.184 | 120.0 |
| N-CA-H(CA) | 292.800 | 116.0 |
| H(CT)-CT-H(CT) | 276.144 | 107.8 |
| CA-CA-H(CA) | 292.800 | 120.0 |
| N-CA-N | 585.760 | 129.1 |

$$V_{proper\ dihedrals}(\phi_{ijkl}) = \sum_{k=0}^{5} C_k(\cos(\psi))^k, \text{ where } \psi = \phi - 180° \quad \text{(S4)}$$

**Tab. S4**: Interaction Torsional Terms

| **Torsion Type** | **C0** (kcal/mol) | **C1** (kcal/mol) | **C2** (kcal/mol) | **C3** (kcal/mol) | **C4** (kcal/mol) | **C5** (kcal/mol) |
|---|---|---|---|---|---|---|
| CA-CA-CA-CA | 30.334 | 0.0 | -30.334 | 0.0 | 0.0 | 0.0 |
| CA-N-CA-CA | 30.334 | 0.0 | -30.334 | 0.0 | 0.0 | 0.0 |

| | | | | | | |
|---|---|---|---|---|---|---|
| N-CA-CA-CA (T1) | 7.079 | 0.0 | -7.079 | 0.0 | 0.1 | 0.0 |
| CA-CA-CA-N (T2) | 9.079 | 0.0 | -9.079 | -0.1 | 0.0 | 0.0 |

$$V_{improper}(\xi_{ijkl}) = \frac{1}{2} k_{\xi} (\xi_{ijkl} - \xi_0)^2 \qquad \text{(S5)}$$

**Tab. S5**: Improper Dihedral Angles

| **Torsion Type** | $\xi_0$ (deg.) | **C** (kcal/mol/rad$^2$) |
|---|---|---|
| CA-CA-CA-CA | 180.0 | 10.460 |
| H(CA)-CA-CA-CA | 180.0 | 10.460 |
| N-CA-CA-CA | 180.0 | 10.460 |
| CA-N-N-CT | 180.0 | 10.460 |

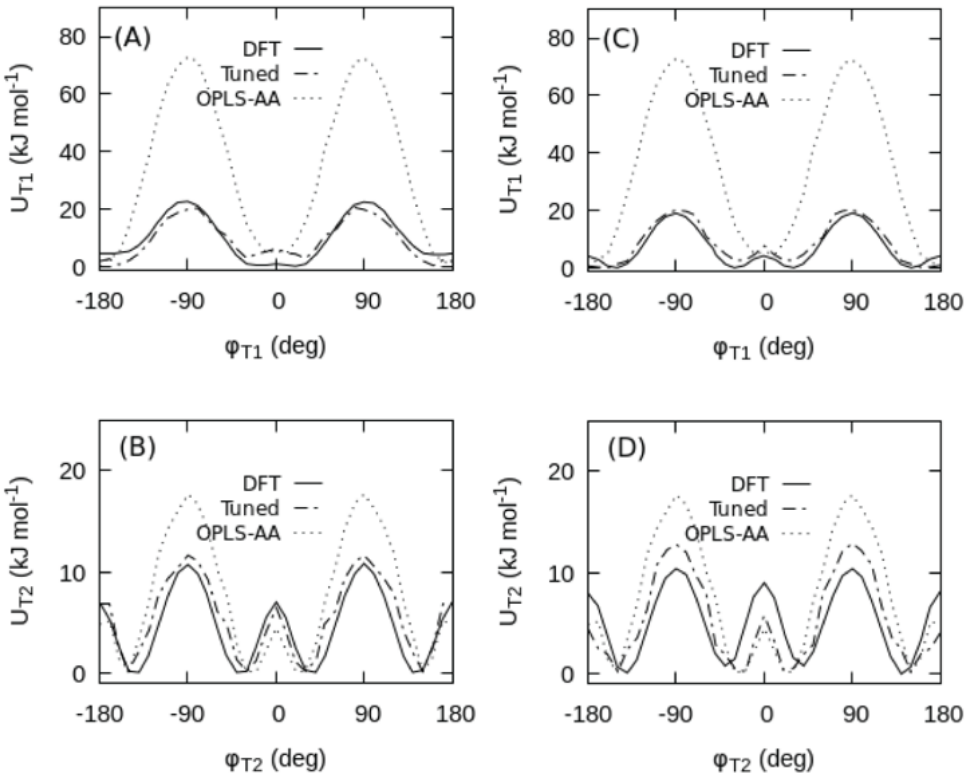


**Figure S2.** Torsional energy profiles for the indicated dihedral angles $\varphi_{T1}$ and $\varphi_{T2}$. Solid lines represent the DFT calculations at PBE0/6-311G* level. Dashed lines represent energy profiles obtained from OPLS-AA parameters, while dashed dotted lines represent energy profiles obtained from the tuned parameters.

# 2. Additional Analysis

## 2.1 Crystalline System of B4PyPTZ

The crystalline structure of B4PyPTZ has been reported by Kido and co-workers[3] and is currently available as crystallographic data in the Cambridge Crystallographic Data Center as publication no. CCDC-1030701. In particular, the unit cell of B4PyPTZ has been found to be monoclinic belonging the space group $P2_1/c$. The lattice constants a = 26.845(6), b = 17.1582(4), c = 26.621(6) Å and $\alpha = 90^o$, $\beta = 98.68^o$ and $\gamma = 90^o$. In Figure S3, the chemical structure of B4PyPTZ is reported.

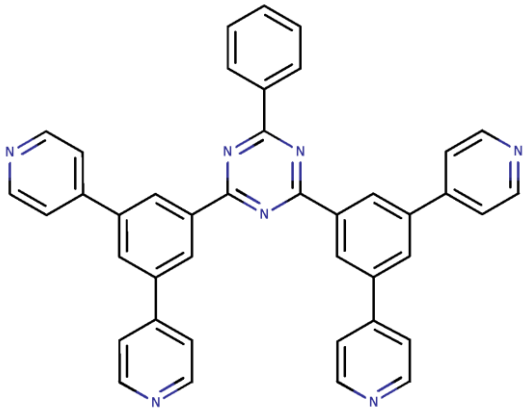

**Figure S3**. Chemical structure of the B4PyPTZ molecule.

By replicating the unit cell of B4PyPTZ, a crystal slab counting 128 molecules was built. In particular, the replicated structure counts 8 columns each one composed of 16 stacked molecules, as shown in Figure S4. The energy of the replicated structure has been minimized by using a steepest-descent algorithm (5000 steps). Then, the minimized configuration was used as initial configuration for a short MD simulation in NVT ensemble (10 ns). After a short NPT equilibration, a long NPT production run has been performed. The mass density has been registered during the simulation, and its time behavior is reported in Figure S5. The average mass density (1278 kg/m$^3$) from MD simulation underestimates the experimental density[3] of about -3.1%. Likewise, the lattice constants are slightly overestimated (+1.9%) even if the crystalline structure is well preserved.

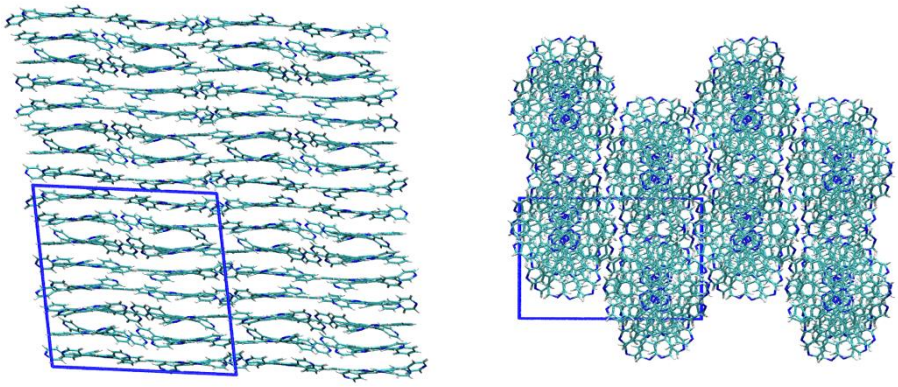

**Figure S4.** Lateral and top view of the replicated B4PyPTZ system. The unit cell (in blue) is over imposed on molecules.

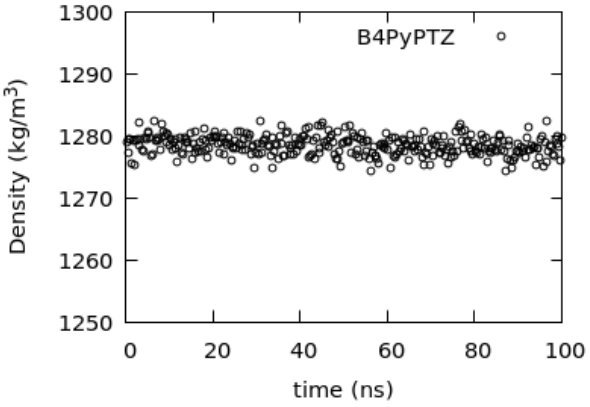


**Figure S5.** Mass density for the crystalline system of B4PyPTZ simulated at 298 K.

In Figure S6, the comparison of X-ray spectrum calculated from the equilibrium configuration from MD and for the replicated initial configuration is reported. As it can be seen, the equilibrium structure from MD simulation retains the main characteristics of the experimental crystal, such as the position of the main peaks and the spacing between them.

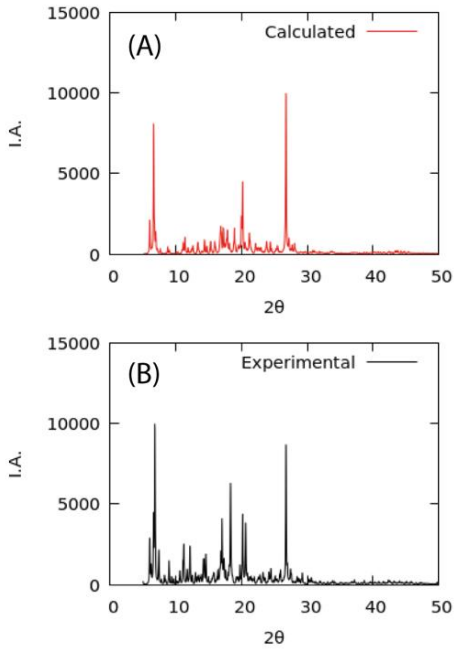


**Figure S6.** X-Ray of B4PyPTZ: (A) spectra computed from long NPT run (100 ns), (B) Experimental.[3] The profiles have been calculated by using CSD Mercury 2.0 code.[4]

## 2.2 Thin Film Preparation

Crystalline B4PyPTZ coordinates were used to build BPyMPM systems. Initial coordinates of B4 molecules are obtained starting from those of B4PyPTZ molecules in the crystalline structure via superposition of the corresponding atoms. The atoms selected for the superposition are indicated in panel A of Figure S7. The superposition is achieved by rigid rotation of the B4 molecules on the B4PyPTZ in the crystalline lattice. In particular, the generated structure must minimize the root-mean-square deviation (RMSD) between BPyMPM and B4PyPTZ sites. To superimpose the two sets of coordinates we adopt the quaternions method reported by Kearsley.[5] Panel B of Figure S7 shows the schematic procedure in which a single column of B4PyPTZ molecule is converted in a column of B4PyMPM. In total, 128 molecules have been replaced in the whole system. The same procedure is applied also for B2 molecules. The energy of the two generated systems has been minimized by performing 500 steps of steepest-descent algorithm. Then, a short NVT simulation (25 ns) has been performed before a production run (100 ns) in NPT ensemble.

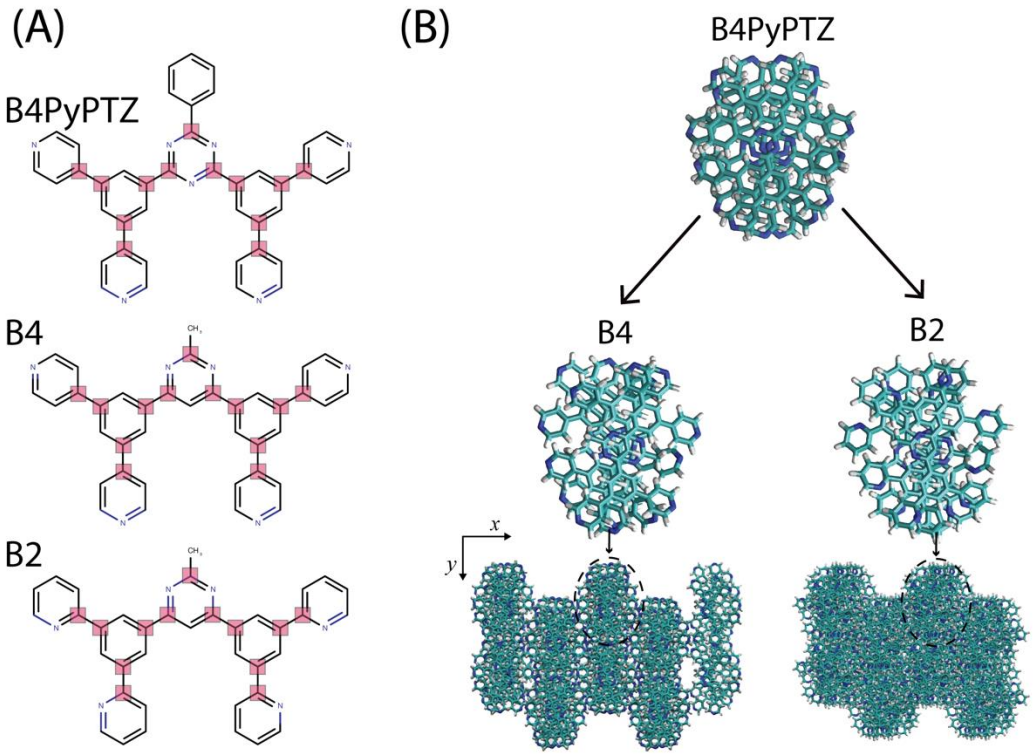


**Figure S7.** (A) Definition of the substitution sites, indicated as red shaded squares, for the B4 and B2 molecules. (B) Scheme of the substitution procedure. In the scheme a column made of B4PyPTZ molecules is converted in B2 and B4, respectively. Then, final systems (each one composed of 128 molecules) are generated.

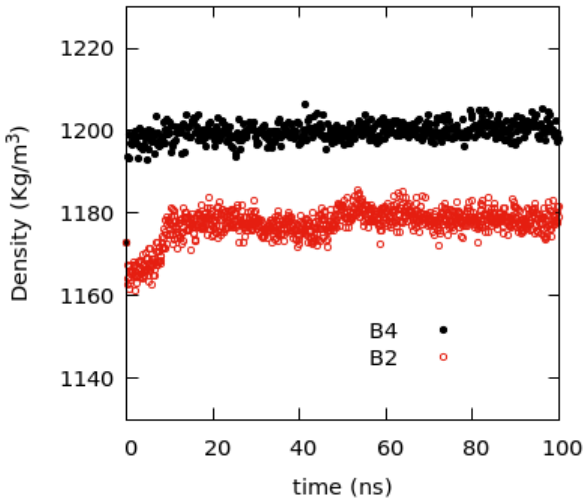


**Figure S8.** Time behavior of mass density for the bulk systems: B4 (black circles) and B2 (red open circles).

## 2.3 Hydrogen Bonds(H-Bonds): adopted Criteria and additional analysis

**2.3.1 H-Bond searching criteria.** Hydrogen bonds are searched and counted when two geometrical conditions are simultaneously satisfied. The first condition is about the distance between the acceptors (A) and the donor (D) which must be shorter than a cut-off distance $r_c$. The second condition is about the angle described by the acceptor-hydrogen-donor, $\theta_{(A-H-D)}$, that must be larger than a cut-off value ($\theta_{cut-off}$). The current literature prescription suggests as cut-off values[6] $r$ = 0.3 nm and $\theta_{(A-H-D)}$ = 120º. However, because the systems we investigated is made of molecules in solid phase, we have tested different cut-off values to verify the correct applicability of the prescribed ones.

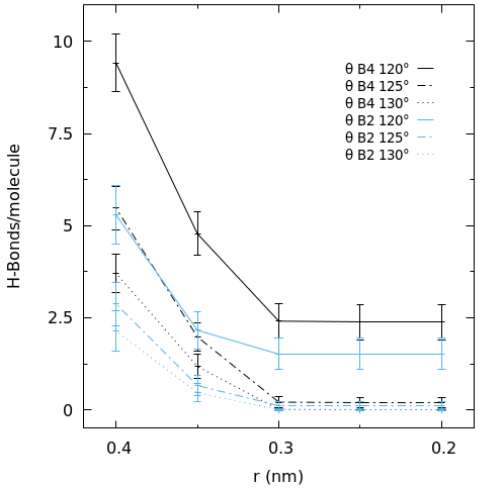


**Figure S9.** Number of H-Bonds per molecule calculated for different distance $r$ and $\theta_{(A-H-D)}$.

As can be seen from the plot in Figure S9, the usual values of $r$ = 0.3 nm and $\theta_{(A-H-D)}$ = 120º give reasonable results in terms of H-Bonds per molecule. Considering that each molecule has 4 nitrogen atoms that could act as acceptors, for a distance $r$ larger than 0.3 nm the number of H-Bonds is inconsistent with that inspected by visualizing the configurations. Similarly, for $\theta_{(A-H-D)}$ larger than 120º, the number of H-Bonds/molecule drastically drops down to ~0., which is in contrast with the experimental evidence of a H-Bond network.[7] For this reasons, we eventually adopted the values proposed in reference [6].

**2.3.2 intra- inter-layer H-Bonds.** The criteria to identify intra- and inter-layer H-Bonds is based on a geometrical distance. If the distance (along normal direction $z$) between donor (D) and the acceptor (A) is lower than the cut-off distance of 0.2 nm, the H-Bond is counted as intra-layer. Instead, for distance D-A larger than 0.2 nm, the H-Bond is counted as inter-layer.

The cut-off distance has been determined by considering the average layer-layer distance computed via density profile. In Figure S10, a scheme illustrating the distance between two layers and the number density profile calculated on the B4PyMPM (film system) are reported.

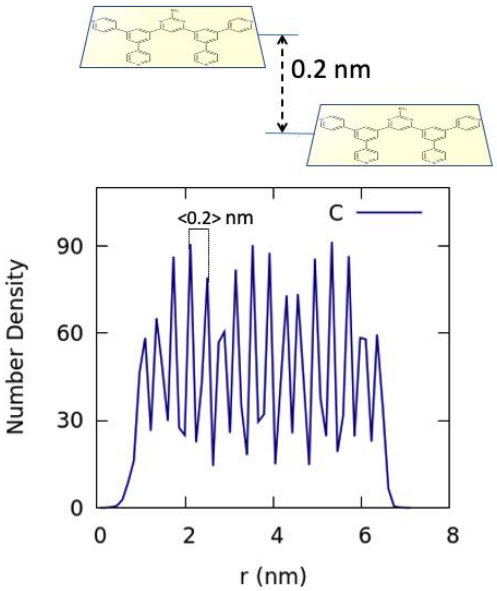


**Figure S10.** (top panel) scheme to show the cut-off distance between two layers. (bottom panel) Number density profile calculated along the normal direction of the layers. The density profile has been calculated averaging the last 35 ns of the production run. Only carbon atoms (CA) have been considered.

**Table S6.** Intra- end inter-layer H-Bond/molecule.

| System | Total No. H-Bond/molecule | H-Bond/molecule intra-layer (*xy*) | H-Bond/molecule inter-layer (*z*) |
|---|---|---|---|
| B4 | 2.42 ± 0.21 | 2.25 ± 0.24 | 0.17 ± 0.17 |
| B2 | 1.49 ± 0.23 | 0.99 ± 0.18 | 0.5 ± 0.31 |

In Table S7, the intra- and inter-layer HBs are listed. We have found that the B4 molecules prefer to form intra-layer HBs (~ 94%), as reported in Table S6. Only the ~ 6% of the HBs are formed perpendicularly to the layers (z direction). Differently, the B2 molecule form ~ 70% of the HBs intra-layer, but a significant ~30% of the total number of HB/molecules is formed between layers (in z direction). This result is a further confirmation of the fact that B4 molecules form, favourably, HBs in 2D dimensions (2.25 HB/molecule intra-layer) with the respect to the B2 (~1 HB/molecule intra-layer).

**2.3.3 Hydrogens atoms involved in the H-Bond formation.** Another important difference between the HBs formed by B4 and B2 molecules is about the hydrogen atoms involved, preferentially, in the HB formation. Following the reviewer suggestion, we tried to identify which hydrogens are more involved in the HB/molecule. To this aim, according to their position in the chemical structure of the B4 or B2 molecules, we identified three different hydrogen types: A, B, and C. In Figure S7, a scheme illustrating the hydrogen type assignment, for both molecules B4 and B2, is reported. In particular, the hydrogens of type A (in blue) belong the external aryl rings (rings 4,5,6,7 in Figure S7), the B type hydrogens (in green) are connected to aryl rings 2 and 3 shown in the of Figure S7, and the C type hydrogen (black) is bonded to the central ring (ring 1 in Figure S7).

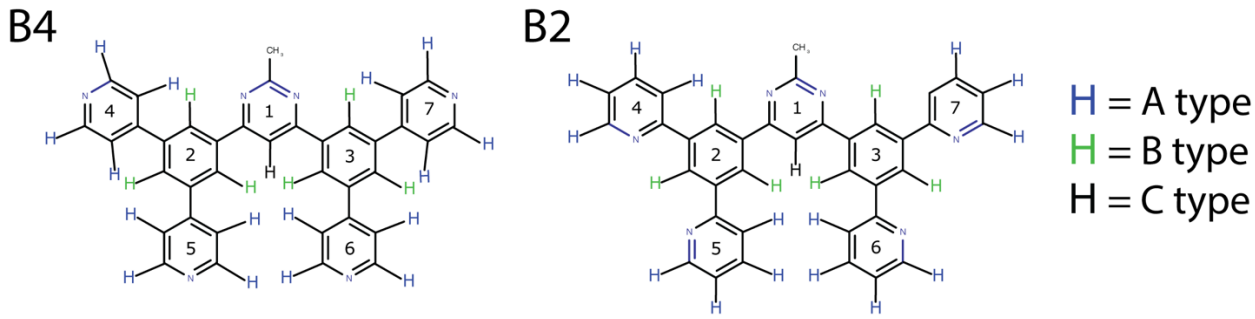


**Figure S11.** Assignment of A, B and C Hydrogen types for the B4 and B2 molecules.

According to the scheme reported in the figure, we computed the total, and partials (for each hydrogen type), numbers of HB/molecule. In Table S7, the results are listed for both molecules.

As general behaviour, for both molecules the hydrogens of type A are the most involved in the HB formation. In the case of B4, almost 81% of HBs are formed with hydrogens of type A (the most external), while ~ 17% of HBs are formed by the B type hydrogens. Only a residual 2% is accountable to the C type. Differently, in the case of B2 molecule, the type A hydrogens are found to form ~ 70% of the HBs (10% lower than B4), while, for the hydrogens of type B the percentage increased from 17% (in case of B4) to 29%. This is mainly due to the fact that hydrogens of type B, in the B2 molecule, have a higher accessible volume with respect to the same hydrogens in the B4 molecules (see the hydrogens between the rings 4, 5 and 6, 7 in the scheme of Figure A2). Lastly, also for the B2 molecule, the C type hydrogen shows a residual ~ 1.3 %.

**Table S7.** Total and partial H-Bonds/molecule.

| System | Total No. H-Bond/molecule | No. of H-Bond/molecule | | |
|---|---|---|---|---|
| | | Type A | Type B | Type C |
| B4 | 2.42 ± 0.21 | 1.95 ± 0.09 | 0.42 ± 0.11 | 0.05 ± 0.18 |
| B2 | 1.49 ± 0.23 | 1.04 ± 0.13 | 0.43 ± 0.28 | 0.02 ± 0.2 |

## 2.4 Additional Analysis on bulk and molecular structures

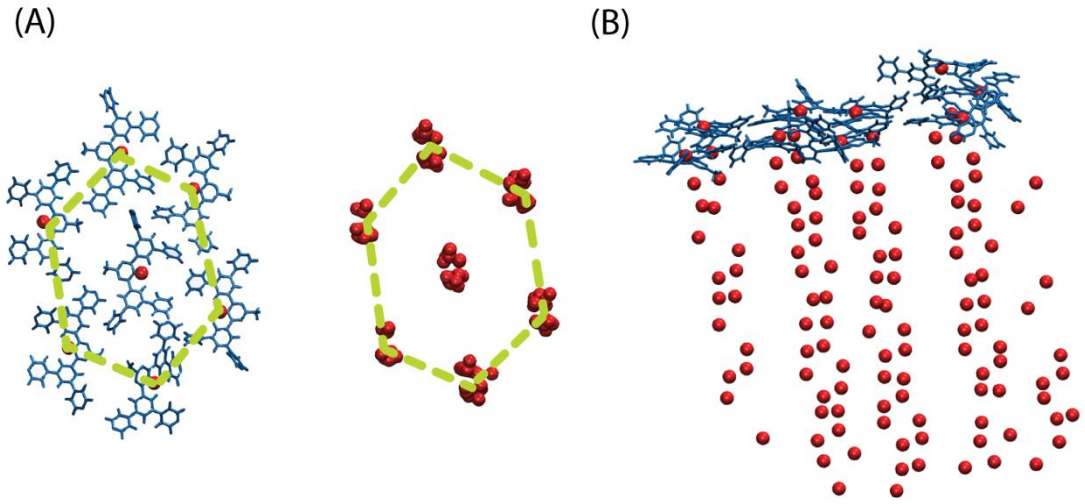


**Figure S12.** (A) top view of B4PyMPM molecules lying in a plane. The red beads represent the hydrogen atom bonded to the central pyrimidine ring. On the right of the same panel, only hydrogens position, for subsequent layers, are reported. The green lines are reported on both snapshots as eye guide to highlight hexagonal packing. (B) lateral view of a section of the B4PyMPM system. Red Beads have the same meaning as in the panel A.

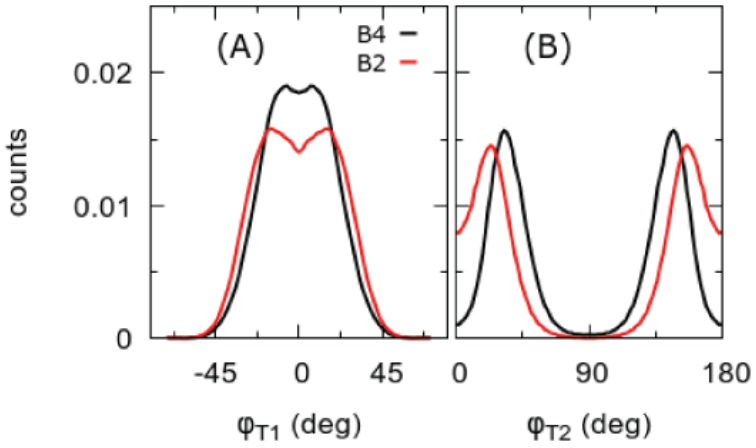


**Figure S13.** Distribution of dihedral angles $\varphi_{T1}$ (A) and $\varphi_{T2}$ (B). The distributions have been calculated by sampling all 128 molecules in each system. The last 50 ns of production runs of the systems (vacuum/film interface) have been considered.

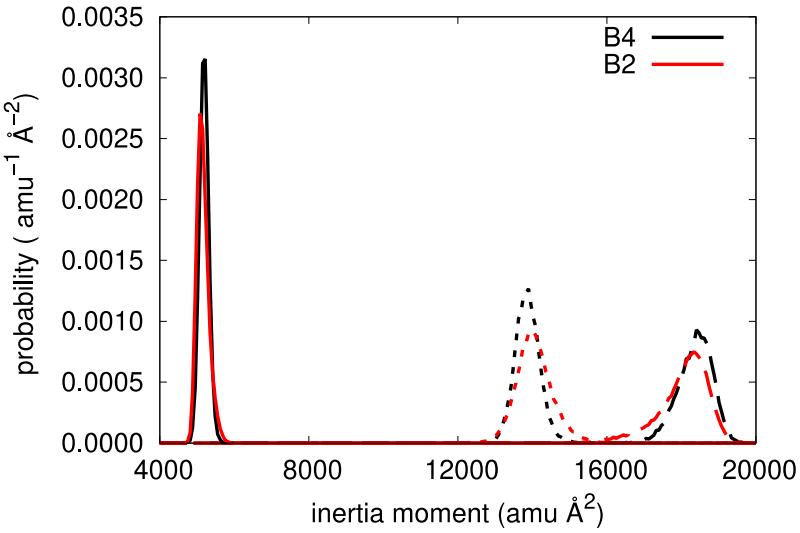


**Figure S14.** Distribution of inertia momentum calculated for B4 (black line) and B2 (red line).

As can be seen from Figure S12, the calculated inertia momentum confirms that both molecules are very similar. In particular, the molecular shape of B4 and B2 is almost coincident, as can be seen from the position of the most intense peak. Only a small difference between the width of the distributions at higher values of the inertia momentum is found.

## 2.5 Additional Charge Transport Calculations

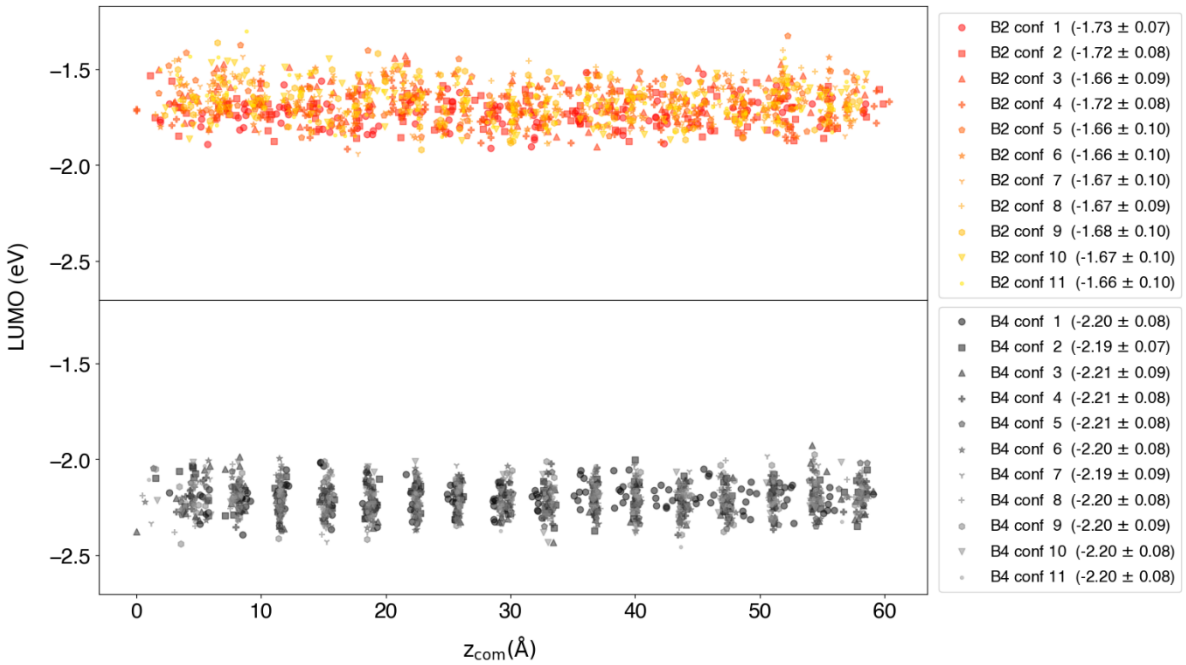


**Figure S15:** Scatter plot of the intramolecular contribution ($E_{LUMO}$) to electron affinities, calculated on 11 different samples for B2 and B4 systems.

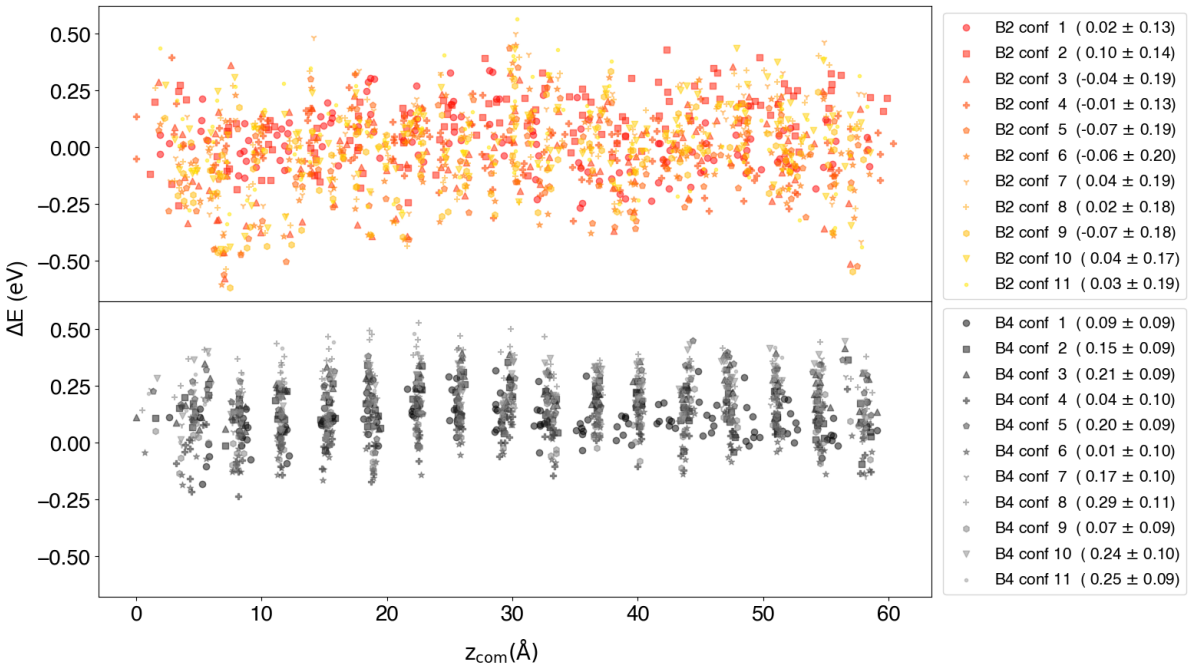


**Figure S16**: Scatter plot of the intermolecular contribution ($\Delta_E$) to electron affinities, calculated on 11 different samples for B2 and B4 systems.

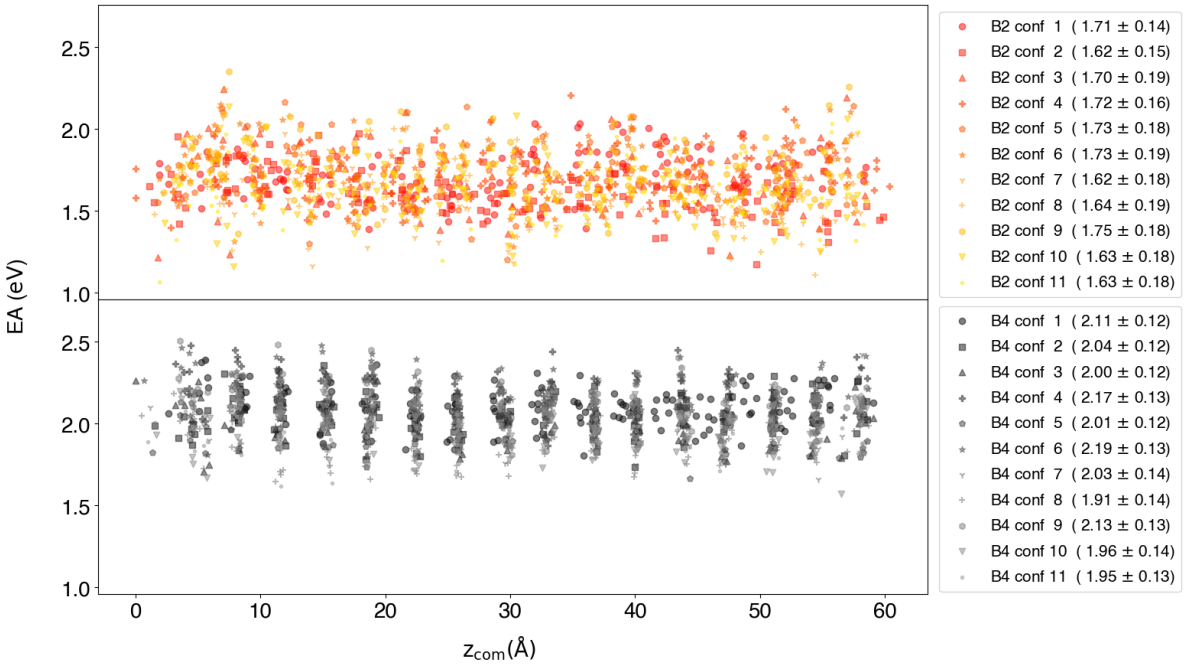


**Figure S17**: Scatter plot of total electron affinities $EA = -(E_{\mathrm{LUMO}} + \Delta_E)$, calculated on 11 different samples for B2 and B4 systems.

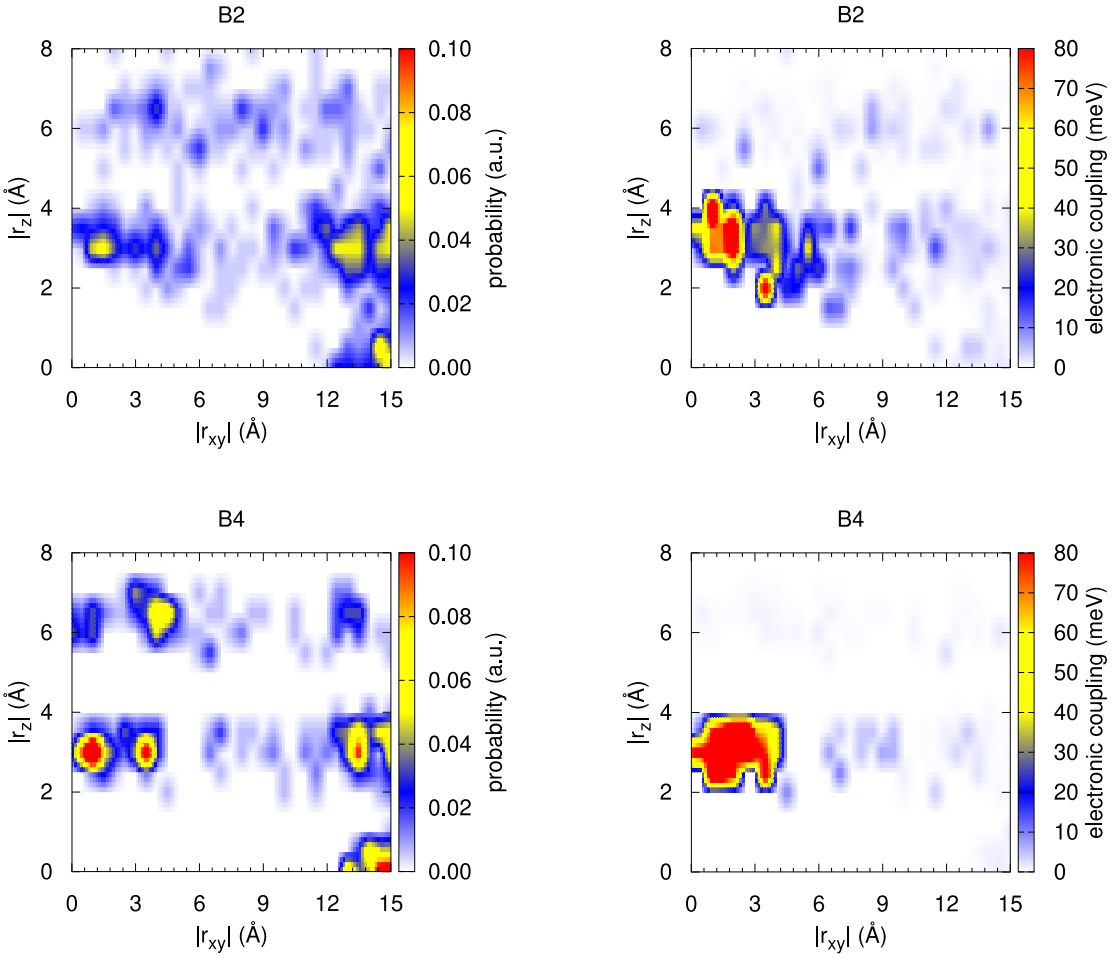


**Figure S18**: Probability of finding a neighbor molecule as a function of the component of the intermolecular vector parallel ($r_z$) and perpendicular ($r_{xy}$) to the stacking direction (left), and (right) corresponding average value of the electronic coupling.

## References:


[1] Chen B., Martin M. G., Siepmann J. I. *J. Phys. Chem. B* **1998**, *102* (14), 2578–2586. https://doi.org/10.1021/jp9801065.

[2] Jorgensen W. L., Mcdonald N. A. *Development of an All-Atom Force Field for Heterocycles. Properties of Liquid Pyridine and Diazenes'*; 1998; Vol. 424.

[3] Watanabe Y., Sasabe H., Yokoyama D., Beppu T., Katagiri H., Pu Y. J., Kido J. *Adv. Opt. Mater.* **2015**, *3* (6), 769–773. https://doi.org/10.1002/adom.201400532.

[4] Macrae C. F., Bruno I. J., Chisholm J. A., Edgington P. R., McCabe P., Pidcock E., Rodriguez-Monge L., Taylor R., van de Streek J., Wood P. A. *J. Appl. Crystallogr.* **2008**, *41* (2), 466–470. https://doi.org/10.1107/S0021889807067908.

[5] Kearsley S. K. *Acta Crystallogr. Sect. A* **1989**, *45* (2), 208–210. https://doi.org/10.1107/S0108767388010128.

[6] van der Spoel D., J. van Maaren P., Larsson P., Tîmneanu N. *J. Phys. Chem. B* **2006**, *110* (9), 4393–4398. https://doi.org/10.1021/jp0572535.

[7] Yokoyama D., Sasabe H., Furukawa Y., Adachi C., Kido J. *Adv. Funct. Mater.* **2011**, *21* (8), 1375–1382. https://doi.org/10.1002/adfm.201001919.